Astron. Astrophys. 250, 220–234 (1991)

ASTRONOMY AND ASTROPHYSICS

Two-dimensional models of the solar chromosphere

I. The Ca II K line as a diagnostic: 1.5-D radiative transfer

S. K. Solanki [1], O. Steiner [1], and H. Uitenbroeck [2,3]

[1] Institute of Astronomy, ETH-Zentrum, CH-8092 Zürich, Switzerland
[2] Sterrekundig Instituut Utrecht, Postbus 80000, NL-3508 TA Utrecht, The Netherlands
[3] Harvard-Smithsonian Center for Astrophysics, 60 Garden Street, Cambridge, MA 02138, USA

Received October 9, 1990; accepted February 2, 1991

Abstract. Profiles of the Ca II K line are calculated for a 5 level atom and partial frequency redistribution along multiple rays (1.5-D) passing through two-dimensional (2-D) MHD models of magnetic flux tubes in the solar atmosphere. Temperature stratifications corresponding to various empirical chromospheric models are incorporated into the models. The influence of a number of model parameters on individual and spatially averaged line profiles is considered in detail. The profiles are also compared with observations. It is found that the present models can, at least qualitatively, reproduce a wide variety of observations if the temperature within the magnetic component lies between that of model F of Vernazza et al. (1981) and of model VALP of Ayres et al. (1986) and if the temperature in the non-magnetic part of the atmosphere corresponds to that of the COOLC model of Ayres et al. The observations that are consistent with such a model include:

1. The spatially averaged Ca II K quiet Sun profile.
2. The spatial scale and the amplitude of horizontal K_2 intensity variations in the quiet Sun (including the network).
3. The qualitative form of the relationship between the K line core intensity and the magnetic flux density in an active region, including the presence of a "basal" flux, i.e. a chromospheric emission in the local absence of a photospheric magnetic field.
4. The presence of a cool fraction of the solar chromosphere with temperatures below 4000 K, as suggested by observations of infrared CO lines.
5. The presence of magnetic canopies in the lower or middle chromosphere of the quiet Sun and the presence of lower lying canopies in active regions.
6. The highly intermittent nature of the photospheric magnetic field.

Points 4 and 6 are a direct consequence of the model input.

Key words: The Sun: chromosphere – The Sun: magnetic fields – Ca II – radiative transfer – line profiles

1. Introduction

The solar chromosphere exhibits a complex structure, as any spectroheliogram or filtergram in Hα or Ca II H or K will confirm. It is difficult to imagine how the wealth of structure and detail seen in such images (e.g. Bray & Loughhead 1974; Bonnet et al. 1980; Athay 1986; Zirin 1988) can be explained by plane-parallel models, such as the empirical models of Gingerich et al. (1971), Ayres & Linsky (1976), Basri et al. (1979), Vernazza et al. (1976, 1981, the last of these is referred to in the following as VAL 81), Gouttebroze et al. (1978) and Maltby et al. (1986), or the theoretical models of Anderson (1989) and Anderson & Athay (1989).

The above models have been highly successful in reproducing spatially averaged properties of the solar chromosphere and have substantially increased our understanding of spatially averaged chromospheric line formation and energy balance (Avrett 1985, 1990). However, spatially resolved observations demand multi *dimensional* models. First steps in this direction were taken by VAL 81, Chapman (1981), Avrett (1985), and Ayres et al. (1986), who constructed multi*component* models of the chromosphere. Although such models may be able to reproduce a larger variety of observations than plane-parallel averaged models, they do not provide any constraints on the geometry and the location of the different components. Also, depending on the type of observations used to construct the multicomponent models, the atmospheric components of the various models are totally different. For example, compare models A′ and F′ of Avrett (1985) with COOLC and FLUXT of Ayres et al. (1986). The former pair of atmospheres reproduces Ca II K variations, the latter infrared CO lines. This criticism is supported by the recent paper of Athay & Dere (1990), who showed that within the constraint of single-dimensionality, observations of EUV lines of O I, C I, and Fe II are not compatible with the models of Ayres et al. (1986) and therefore with spectra of CO lines.

In the present and in following papers we take the next logical step to overcome these shortcomings and consider proper 2-D models. To this end we explore and apply spectral diagnostics based on Ca II K and 1.5-D radiative transfer in the present paper. These calculations must be considered exploratory in nature and we do not at this stage derive a detailed empirical 2-D model. In future investigations we also plan to develop self-consistent models including more realistic contributions to the energy balance. Earlier 2-D models with sufficient sophistication to serve as the basis of line profile calculations have either concentrated on the photosphere (e.g. Knölker et al. 1990; Steiner 1990; Bünte et al. 1991) or on the transition region and the upper chromosphere (e.g. Gabriel 1976; Fiedler & Cally 1990), whereas we attempt to obtain a self-consistent model valid in both the photosphere and the chromosphere.

Send offprint requests to: S. K. Solanki

A successful 2-D model of the chromosphere must at least ualitatively satisfy the following, obviously incomplete, list of asic observations:

1. The spatially averaged spectrum resulting from the 2-D nodel should reproduce spatially averaged observations, or quivalently, spectra produced by plane-parallel empirical nodels, e.g. the quiet Sun model of Maltby et al. (1986).

2. The small-scale spatial structure observed in temperature ensitive lines (Ca II H+K, Mg II h+k, Lyα, e.g. Bonnet et al. 978, 1980) or in the continuum (400–1700 Å e.g., VAL 81, 00 μm, e.g. Lindsey et al. 1990) should be mimicked by brightness tructures at similar scales in synthetic spectra.

3. The correlation between the photospheric magnetic flux (or ather the circular polarization) and chromospheric temperature ndicators, like the Ca II K_2 brightness (Skumanich et al. 1975; Schrijver et al. 1989) or the 1600 Å continuum (Cook & Ewing 1990), should be present in the models.[1] A "basal" flux of Ca II core emission uncorrelated with the local photospheric flux density should also be present (Schrijver 1987; Schrijver et al. 1989).

4. The models should allow for the presence of cool material in the lower chromosphere required to satisfy observations of CO lines (Ayres & Testerman 1981; Ayres et al. 1986).

5. The magnetic field in the models should form a canopy in the lower chromosphere for quiet regions or in the upper photosphere for active regions. The presence of a low lying canopy is indicated by magnetograms obtained near the limb (Giovanelli 1980; Giovanelli & Jones 1982; Jones & Giovanelli 1983).

6. Finally, no model of the chromosphere is complete without including the photosphere where the continuum and the wings of most chromospheric lines are formed. In particular the photospheric part of a 2-D model must take the highly intermittent nature of the photospheric magnetic field into account (e.g. Stenflo 1989).

Currently there is only a single type of model that can simultaneously satisfy points 4, 5, and 6. This is a flux tube model with a hot magnetic component surrounded by and overlying a cool magnetic gas without a chromospheric temperature rise (Solanki & Steiner 1990). We feel that this is currently also the only type of model that can resolve the contradiction between the work of Ayres et al. (1986), who find that close to 90% of the surface does not show a temperature rise in the lower chromosphere, and that of Athay & Dere (1990), who conclude that a chromospheric temperature rise is present over 90% of the solar surface. In the present paper we test whether this type of model can also satisfy the observational constraints listed under points 1, 2, and 3, at least within the limits of Ca II K line diagnostics. By restricting ourselves to the Ca II K line we also restrict ourselves to the lower and middle chromosphere. We explore the diagnostic potential of this line within the framework of 2-D MHD models. We choose empirically determined 1-D atmospheres for both components and test how they fare when incorporated into otherwise self-consistent 2-D models. A similar approach, namely the incorporation of 1-D atmospheres into a 2-D model, has already been successfully applied in the photosphere (e.g. Solanki 1989; Keller et al. 1990).

The observational constraints listed under points 4, 5 and 6 are independent of our choice of spectral line. However, points 1, 2, and 3 must be specified more precisely to the aims of the present paper. The precise observational constraints are:

1. The Ca II K_2 intensity averaged over all the rays passing through the 2-D model should be similar to that produced by the Maltby et al. (1986) model, if the magnetic filling factor α^* in the 2-D model is sufficiently small (we choose $\alpha^* \approx 0.5\%$ at the quiet Sun $\tau_{5000} = 1$ level).

2. The Ca II K_2 emission from the magnetic network should vary on a spatial scale of approximately 1″ (cf. Fig. 22 of Bonnet et al. 1978 for Ca II H, or Fig. 3 of Cram & Damé 1983). The distribution of K_2 intensities and, e.g., the intensity difference between supergranule cell centers and the network at 1″ resolution has been given by Grossmann-Doerth et al. (1974).

3. The intensity of the K line core, averaged over an area of approximately $2000 \times 2000\,\mathrm{km}^2$, should show a well defined dependence on the total magnetic flux in the same area (Skumanich et al. 1975; Schrijver et al. 1989). For small filling factors (for a fixed field strength the magnetic flux is proportional to the magnetic filling factor, α^* at $z = 0$) the K line core intensity should increase rapidly with α^*, while for larger α^* it should begin to saturate, i.e. become independent of α^* (Schrijver et al. 1989). Even if no photospheric magnetic flux is present in the spatial resolution element, the Ca II K line core intensity should not fall below a certain "basal" value (Schrijver 1987; Schrijver et al. 1989).

2. Hydromagnetic model

For the hydromagnetic calculations the solar atmosphere is assumed to consist of two basic components, a magnetic component whose outer boundary has the shape of a wine glass and a non-magnetic component filling the rest of space. The vertical stem of the wine glass represents a photospheric flux tube, while the upper part, lying above the merging height h_m of the tubes, is composed of a more or less uniform field. The merging height h_m is defined as the height at which two neighbouring flux tubes meet. Above it the magnetic field fills all of the available space. The part of the model at intermediate heights, where the main expansion of the field takes place, is often termed the magnetic canopy. The temperature and pressure stratification in the two components are taken from separate empirical models. The magnetohydrostatic equations are then solved for the rotationally symmetric magnetic field using an iterative technique and assuming the field to be bounded by a current sheet. The other input parameters of the model need only be specified at a single height, $z = 0$ (corresponding to $\tau_{5000} \approx 1$ in the quiet Sun). They are the field strength B^* at the axis of symmetry, the filling factor α^* and the flux tube radius R^* (* represents quantities at $z = 0$). More details on the code and the properties of the solutions are given by Steiner et al. (1986), Steiner & Pizzo (1989), and Solanki & Steiner (1990), where figures of the resulting structures may also be found (cf. Fig. 2).

One of the most restrictive assumptions made here is magnetohydrostatic equilibrium, i.e. the neglect of all dynamical effects. Velocities may become of the order of the sound speed in the chromosphere, so that their influence ought to be taken into account explicitly and not simply through the turbulent pressure. However, we feel that dynamical calculations at the present stage would make it more difficult to distinguish the effects of 2-dimensionality, which we are mainly interested in. We also simplify the fine structure of the individual network points, each of which is in reality probably composed of a group of individual flux tubes, by representing a whole network point by a single small flux tube. Without this assumption a full 3-D calculation would be required. Finally, in the present investigation the temperature and

[1] The intensity minima in the wings of the K line are designated by K_1, the emission peaks by K_2, and the central minimum by K_3.

Table 1. Summary of calculated 2-D models

Model name	Magnetic atmosphere	Non-magnetic atmosphere	α^*	B^* (G)	β^*	h_m (km)
A	FLUXT	COOLC	0.005	1500	0.217	910
B	FLUXT	COOLC	0.005	1600	0.065	1020
C	FLUXT	COOLC	0.15	1630	0.024	445
D	FLUXT	COOLC	0.05	1630	0.024	700
E	VALP	COOLC	0.005	1500	0.199	990
F	VALP	COOLC	0.005	1600	0.058	1100
G	VALP	COOLC	0.005	1630	0.021	1155
H	VALP	COOLC	0.05	1630	0.021	710
I	VALP	COOLC	0.15	1630	0.021	445
J	VALF	COOLC	0.005	1500	0.210	1140
K	VALF	COOLC	0.005	1600	0.066	1180
L	VALF	COOLC	0.005	1630	0.025	1210
M	VALF	COOLC	0.05	1630	0.025	710
N	VALF	COOLC	0.15	1630	0.025	450
O	C′	C′	0.005	1500	0.295	1505
P	C′	C′	0.005	1600	0.130	1510
Q	C′	COOLC	0.005	1500	0.218	1150
R	C′	COOLC	0.005	1600	0.065	1195
S	C′	COOLC	0.05	1630	0.025	715
T	C′	COOLC	0.15	1630	0.025	450

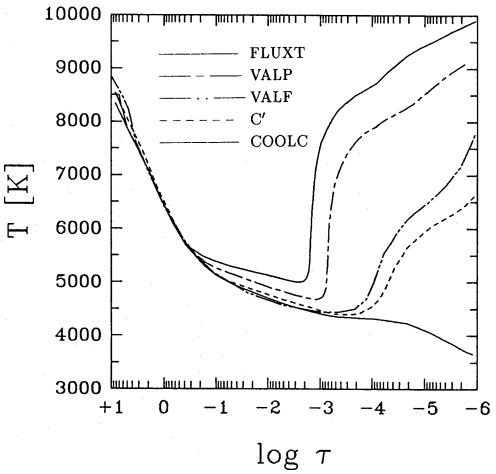

Fig. 1. Temperature, T, vs. logarithmic continuum optical depth at 5000 Å $\log \tau$, for the five empirical atmospheres used in the present investigation. Upper solid curve: FLUXT, dot-dashed curve: VALP, double-dot-dashed curve VALF, dashed curve: C′, lower solid curve: COOLC

all other physical parameters are not allowed to vary horizontally, except at the boundary of the magnetic field, where a jump in these quantities is present. This simplification has the advantage that we can make use of empirical atmospheres for both components. It is clear that a hot flux tube atmosphere interacts with its cool surroundings below the merging height, but this interaction can only be addressed with a fully multidimensional treatment of the radiative transfer which is not within the scope of the present paper. We expect that such a treatment will give rise to a transition layer of a certain thickness across the flux tube surface with a smoothly changing temperature.

As far as the parameterisation is concerned we follow the procedure outlined by Solanki & Steiner (1990), but obtain the pressure difference between the magnetic and the non-magnetic parts of the atmosphere in a different manner. Whereas Solanki & Steiner (1990) simply multiplied the gas pressure at the tube axis by a given factor to achieve horizontal pressure balance, we instead shift the flux tube atmosphere as a whole downwards until $\Delta p = B^2/8\pi$ is achieved at the surface of the flux tube for a field strength B^* specified at $z = 0$ according to Table 1. This relatively minor innovation has the major advantage that the temperature $T(\tau)$ and the electron pressure $p_e(\tau)$ as a function of continuum optical depth τ are not affected by the choice of the field strength. Therefore, the spectrum arising from the axis of symmetry of the 2-D model corresponds exactly to the spectrum arising from the original empirical model. Consequently this step allows us to examine the effects of the 2-D geometry with the least amount of interference from other effects. The merging height h_m of the tubes is affected only slightly by the above change.

One of the following empirical atmospheric models, the temperature stratifications of all of which are plotted vs. continuum optical depth τ_{5000} in Fig. 1, constitutes the magnetic component of each of the 2-D models:

1. C′, the quiet Sun model published by Maltby et al. (1986). This is a single-component model based on quiet Sun continuum and line spectra. More details on its construction have been given by Avrett (1985). It serves, for the purposes of the present investigation, as the representative of a whole group of quiet Sun models, for example VAL 76, VAL 81, the HSRA (Gingerich et al. 1971), Ayres & Linsky (1976), and Basri et al. (1978).

2. FLUXT of Ayres et al. (1986). This is a flux tube model with a very steep temperature rise and correspondingly hot chromosphere. It produces a strong Ca II K_2 peak. In a 2-component model Ayres et al. (1986) were able to reproduce the average quiet Sun profile of Ca II K by combining this model, with a small filling factor, with the COOLC model (see below). The FLUXT model is similar to the flux tube atmosphere proposed by Chapman (1981).

3. VALP of Ayres et al. (1986). This single-component plage model was derived by fitting Ca II K profiles observed in active region plages. Its temperature structure lies approximately in the middle, between that of FLUXT and C′. Comparison with VALF (see below) suggests that it must be considered a hot 1-D single-component plage model. VALP is similar to, but slightly hotter than the average plage model plotted by Chapman (1981). It is the hottest single-component empirical plage model we have found in the literature and may be considered an upper limit to average plage temperatures.

4. VALF of VAL 81. A model of bright network points, constructed under the assumption that these have been spatially resolved in the Skylab observations. Its similarity to the single-component homogeneous plage models of Lemaire et al. (1981) and Shine & Linsky (1974) implies that it may also be considered a single-component plage model and it serves as a representative for the other two models. Since it is considerably cooler than VALP in the chromosphere, we take it to represent a lower limit to the average plage models.

For the non-magnetic atmosphere, besides C′ of Maltby et al. (1986), we have used:

5. COOLC of Ayres et al. (1986). A cool model of the non-magnetic atmosphere without a chromospheric temperature rise. The chromospheric part of the model is based on observations of the CO fundamental and first-overtone vibration-rotation bands. It is relatively similar to, although slightly warmer in the chromosphere than the NLTE line blanketed radiative equilibrium model of Anderson (1989), which includes cooling by the CO molecule.

A list of all the 2-D models calculated using various combinations of these five empirical atmospheres is presented in Table 1. As can be seen from the table, the field strength at the axis B^* and the filling factor α^* have been varied, but only a single radius $R^* = 100$ km has been considered; firstly because observations suggest it is a reasonable value (e.g. Von der Lühe 1989; Zayer et al. 1989), secondly, since the shape of the magnetic boundary and in particular the merging height depends only slightly on R^*/α^* (Solanki & Steiner 1990). In Table 1 β^* is the plasma β at $z = 0$: $\beta^* = 8\pi P_m^*/B^{*2}$ (P_m^* is the gas pressure in the magnetic component at $z = 0$) and h_m is the height at which neighbouring flux tubes merge. The values for the input parameters (B^*, α^*) have been carefully chosen to encompass the observed values following, e.g. Zayer et al. (1990). The photospheric temperatures of the models used here are of roughly similar magnitude as the temperatures of the empirical models of Solanki (1986), Keller et al. (1990), and Zayer et al. (1990).

An additional free parameter of importance for the radiative transfer calculations is the microturbulence velocity ξ_{mic}. For most models different values have been tried: $\xi_{mic} = 2, 4, 6\,\mathrm{km\,s^{-1}}$ independent of height and a ξ_{mic}, which we call VAL-like. It is a schematisation of the VAL 81 turbulence. It assumes that ξ_{mic} is constant at $9\,\mathrm{km\,s^{-1}}$ above $\log \tau_{5000} = -6.5$, decreases linearly in $\log \tau_{5000}$ to $2\,\mathrm{km\,s^{-1}}$ at $\log \tau_{5000} = -3.2$, and remains constant below that height. Unless explicitly mentioned a VAL-like microturbulence is used. In general when a direct comparison of line profiles is made then they are additionally broadened by a macroturbulence ξ_{mac}.

3. Atomic model and radiative transfer

3.1. Atomic model

All line profiles presented in this paper are computed with a five level plus continuum representation of the Ca^+ ion. This includes the $4s^2\,S_{1/2}$ ground level, the two metastable $3d^2\,D_{3/2}$ and $3d^2\,D_{5/2}$ levels and the $4p^2\,P_{1/2}$ and $4p^2\,P_{3/2}$ levels. In the solar atmosphere these five levels are sufficient to provide an accurate description of the physics of formation of the five most important Ca II lines because the next lowest level ($5s$) is more than 3.3 eV away. We include all five important radiative transitions, viz. the H and K resonance lines at 393.4 and 396.8 nm and the infrared triplet lines at 849.8, 854.2 and 866.2 nm and allow for non-LTE effects in each of them. We adopt the collisional and radiative rates and Van der Waals broadening parameters of Shine & Linsky (1974).

To save computer time partial redistribution (PR) effects are only included in the K line. This is a good approximation in the context of radiative transfer modeling in the solar atmosphere, as long as we are only interested in the formation of the K line. The main reason is that PR has little effect on the overall radiative rates; these being largely determined by intensities in the line cores. PR effects in the infrared lines are negligible anyhow because these lines thermalize much deeper in the atmosphere where collisions dominate over scattering. Therefore, the population number of the upper level of the K line ($4p^2\,P_{3/2}$) changes little whether we include PR effects in the other lines or not. Effects of coherent photon conversion (cross redistribution) can also be neglected in the case of the solar Ca lines (Uitenbroek 1989a). In the hot flux tube models under study the electron densities may be one or two orders of magnitude larger than in the quiet Sun models, reducing the importance of scattering. Therefore, the effects of coherent conversion will be even smaller than in the cases investigated by Uitenbroek (1989a).

The bound-free radiative transitions are all treated with fixed radiation temperatures T_{rad}. We assume that the ionisation temperature follows the photospheric electron temperature outwards down to T_{rad} and remains constant at this value higher up in the atmosphere. The radiation temperatures are taken from Shine & Linsky. Because the atmospheric models we study here have similar photospheric temperature stratifications, we feel that it is a good approximation to use the same radiation temperatures in all cases. The only possible exception is a thin ring around each flux tube, where the hot wall radiates more strongly. However, we feel that the walls in our models are too hot (since we have not changed the temperature structure to correspond to the surroundings in the sub-photosphere, as would happen if horizontal radiative transfer were to be included; e.g. Steiner & Stenflo 1990; Grossmann-Doerth et al. 1989). A fixed T_{rad} is therefore a better representation of reality. Ionisation to Ca III only becomes important in the higher layers of the atmosphere where most parts of the K line are already optically thin. Therefore, the precise ionisation mechanism has little effect on the emergent line profile.

3.2. Radiative transfer

The balance of the population numbers between the different atomic levels in each of the models is set by the collisional and radiative rates between them. The radiative rates depend on the specific intensities, which are set by the opacity and source function at many frequencies and depths. The source function and opacity depend in turn on the population numbers, making the multilevel transfer problem a nonlinear one that can in general only be solved with an iterative procedure. To solve the coupled equations of statistical equilibrium and radiative transfer along each ray we use an approximate lambda operator scheme (Uitenbroek 1989a). This method includes the effects of partial frequency redistribution (PR) into the scheme formulated by Scharmer & Carlsson (1985) for multilevel radiative transfer with complete frequency redistribution (CR).

Partial frequency redistribution describes the possible coherence between the incoming and outgoing frequency of a scattered photon. The PR line source function is no longer frequency independent but contains a frequency dependent part that describes the coherent scattering in the line. This adds to the nonlinearity of the transfer problem making it harder to solve than the corresponding CR problem. Moreover, the line source function at one frequency now depends on the intensities at all other frequencies in the line making the problem more non-local and linearisation of the rate equations less straightforward. We give a short review of the method here.

Suppose we have an intermediate result in the iterative process, i.e. estimates of population numbers n_i for all relevant atomic levels and intensities $I_{\nu\mu}$ for all frequencies ν and angles μ. The exact expression for the line source function is used to infer intensities and radiative transition rates from this pertinent solution. These rates are then entered into the equation of statistical equilibrium or rate equation, which will in general not be identically satisfied by this solution indicating that it is not yet consistent with both radiative transfer and statistical equilibrium. Approximate corrections to the intermediate solution can be evaluated by inverting the linearized statistical equilibrium equations (the approximate lambda operator) with the unbalance of the rate equations as a driving term. This process is repeated until

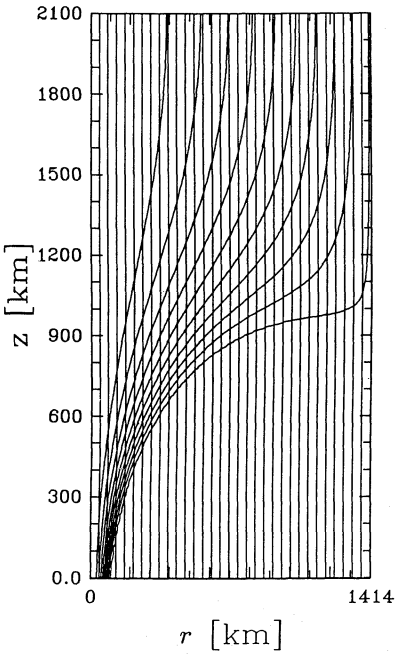

Fig. 2. Selected field lines of a model flux tube superimposed on the rays along which the spectra are calculated. The vertical axis denotes height, z, above the $\tau = 1$ level in the COOLC atmosphere, the horizontal axis denotes the radial distance, r, from the axis of symmetry of the flux tube. Plotted is a tube with a filling factor of 0.5% (model B). The rays are represented by vertical lines

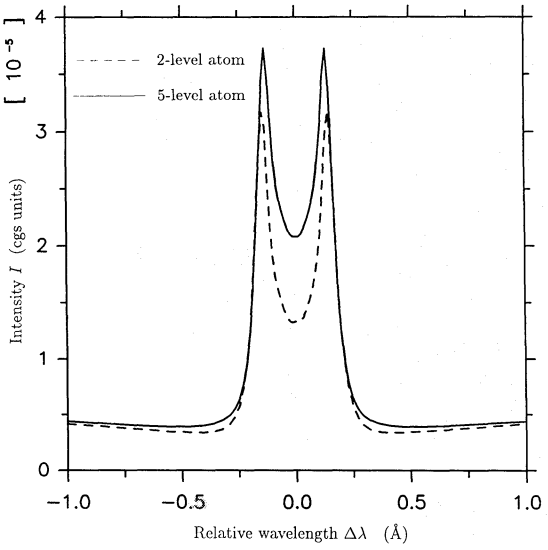

Fig. 3. Comparison of profiles of the K line core calculated for a FLUXT atmosphere using a 5-level atom (solid) with profiles calculated using a 2-level atom (dashed). ξ_{mic} is VAL-like

the relative corrections in the population numbers and mean intensities become smaller than a predefined small number in all transitions.

The scattering part of the PR line source function depends on the intensity in the line, even on the intensities in other lines when coherent conversion processes are important. So it tends to lag one iteration behind, since these intensities are not yet available at the moment the source function is evaluated. Therefore, the method includes for each PR line an extra loop over frequency and angle to update the specific intensity, while keeping the population numbers fixed.

The evaluation of the scattering integral, the contribution o coherent scattering to the PR source function, poses a numerica problem. The integration over the redistribution function has t be performed on a much finer frequency grid than that on whic the radiative transfer problem is solved because the redistributio function varies much more strongly with frequency than th specific intensity. We use a numerically expedient approximatio of the R_{II} redistribution function due to Gouttebroze (1986) an interpolate the specific intensity with cubic splines as described b Uitenbroek (1989b).

3.3. Comparison with a two-level representation

The classical multicomponent approach neglects the effects of the geometry of inhomogeneities in an atmosphere and treats its components as individual plane-parallel atmospheres, with no coupling at all between them. This method was used by Ayres et al. (1986). These authors proposed a two-component model for the solar atmosphere and determined the filling factor of their hot (FLUXT) component, embedded in a cool (COOLC) component, by matching a linear combination of the respective profiles with a quiet-Sun and with a moderate plage profile.

To compare our results with those of Ayres et al. we calculated line profiles, both with our five-level representation for the Ca^+ ion, and the two-level representation used by Ayres et al. (1986). These calculations clearly show that it is important to include all five levels even in a comparative study. Figure 3 illustrates the difference between the two representations for the FLUXT component. The K_2 emission in the five-level case is much stronger than in the two-level case. The reason for this is the strong collisional coupling of the $4p$ levels to the ground level via the $3d$ levels due to the high electron density in the hot component. This coupling prevents a decrease of the $4p$ departure coefficients which normally occurs due to photon losses in the infrared lines in the lower chromosphere and even in the H and K lines higher up. The upper level (b_u) and lower level (b_l) departure coefficients of a line are approximately related to the line source function by $S_L \simeq b_u/b_l B_\nu$, where B_ν is the Planck function (e.g. Athay 1972). By contrast, in a quiet-Sun atmosphere the coupling between $4p$ and $3d$ is, to a much larger part, due to radiative coupling by the infrared triplet lines. In that case the resonance-line upper-level departure coefficients already decrease before these lines dethermalize due to the photon losses in the subordinate lines, causing the emission to be lower in the case of the five-level representation rather than higher. Note that the K_2 emission we obtain with the 2-level + continuum model atom is equal to the emission in Fig. 13 of Ayres et al. (1986) to within a few percent if a similar macroturbulence is applied.

3.4. Multidimensional or multicomponent transfer?

Present limitations in our computer codes do not allow us to treat an inhomogeneous atmosphere with true multidimensional radiative transfer while simultaneously using many levels and partial redistribution. Currently we must simplify either the geometry or else the physics (for instance by taking a two-level representation for the Ca^+ ion and using complete redistribution) of the line transfer problem. We choose the former option because we feel that the horizontal dimensions of the structures we are interested in are sufficiently large for lateral transfer effects not to play an

mportant role. The main reasons for this are the exponential stratification of density (and opacity) in both the tube and the outer atmosphere, and the flaring out of the tube near the thermalisation height of the K line. Tests we have done to compare results of two-level atom computations with our full five-level setup indicate that two levels are not sufficient to give an accurate description of the K-line formation (see Sect. 3.3). We feel that computational results are more suitable for comparison with observations when the more realistic five-level representation, including PR effects, can be employed even at the necessary cost of a simpler geometry (cf. Sect. 3.3).

We take the geometry of the problem (an axially symmetric magnetic field expanding with height) into account in the following manner: We trace a number of vertical rays (16 if $\alpha^* \geqq 0.05$ and 32 if $\alpha^* < 0.05$) through the 2-D MHD model. One ray is placed at the tube axis, and subsequent rays are placed parallel to the axis at progressively larger distances (see Fig. 2). The radiative transfer equations are then solved along each of the rays separately, not taking the exchange of radiation between the different rays into account. The source function in each ray, however, is consistent with the vertical structure of the atmosphere at that specific distance from the flux tube axis. Each ray is thus treated as if it were a one-dimensional plane-parallel, homogeneous atmosphere. In this way we carry out multicomponent rather than two-dimensional (2-D) radiative transfer. This approach is often called 1.5-D radiative transfer. All line profile calculations refer to the centre of the solar disk.

It remains difficult to assess the validity of our multicomponent approximation, since we cannot compare our results with more exact methods. The best we can do at the moment is to estimate the importance of lateral transfer effects by comparing with published estimates. Structures with a horizontal scale of less than roughly an opacity scale height in an exponentially stratified atmosphere may show multidimensional transfer effects. This can be understood with the following simple line of reasoning due to Jones (1986). Let the opacity be given by $\kappa(z) = \kappa_0 \exp(-z/H)$, for $z \leqq 0$ and $\kappa(z) = 0$, for $z > 0$, where z is the height in the atmosphere. Then at great depth (several scale heights from the surface) $\tau(z) \simeq H\kappa(z)$. The optical extent of a structure with horizontal diameter L at depth z is: $L\kappa(z) = (L/H)\tau(z)$. Horizontal transport can only become important as the photon escape probability in the lateral directions is equal to or larger than the probability of vertical escape. So $L/H\tau(z)$ has to be less than or equal to $\tau(z)$ or simply $L \leqq H$. According to more refined analyses (e.g. Stenholm & Stenflo 1977, 1978; Mihalas et al. 1978; Jones & Skumanich 1980; Jones 1986; Trujillo-Bueno & Kneer 1987) this estimate appears too rough. We discuss a few examples of better estimates here.

Avrett & Loeser (1971) present multidimensional calculations of an array of hexagonal tubes in a solar-like atmosphere. Assuming both the tubes and the surrounding atmosphere to be homogeneous, and the source functions to be piecewise linear, they were able to include the horizontal radiative interaction between the two components. They used a two-level atom with the properties of the K-line in the solar atmosphere ($\varepsilon = 2.0\ 10^{-4}$) and treated both variations in opacity and variations in the thermal source term. Their Figs. 4–10 show that lateral transfer between the two components is important only for tube diameters of less than 4–5 opacity scale heights H (constant and equal to 110 km in both components). Moreover, these effects only occur above the thermalisation depth Λ of the line ($\Lambda \simeq 1/\varepsilon$ for a Doppler profile, where ε is the collisional thermalisation parameter of the source function).

The lower limit of $5H$ for two-component behaviour agrees very well with that of Owocki & Auer (1980), who, on the basis of photon diffusion arguments, find that lateral transport may become important for horizontal dimensions $L \leqq H \ln \sqrt{\Lambda}$. They also compare true two-dimensional transfer, using a code developed by Mihalas et al. (1978), with two-component calculations and conclude that the Ca wings show only slight horizontal transfer effects even in structures with horizontal scales approaching an opacity scale height. This confirms the conclusions of Mihalas et al. (1978) who find no evidence for lateral transfer in exponential atmospheres on horizontal scales of more than an opacity scale height. In some cases, however, they found slight multidimensional transfer effects in a free standing slab for depths less than the thermalisation depth.

Jones (1986) published a series of graphs of modulation functions, describing the response of a two level atom source function to periodic horizontal thermal perturbations. He found that in an exponentially stratified atmosphere lateral transfer effects have to be included for temperature inhomogeneities with a horizontal wave number of $k > H^{-1}$. For strong lines, such as the K-line the transition from multicomponent to multidimensional behaviour already starts at horizontal dimensions of five scale heights, in good agreement with the estimates cited above.

When we look at Fig. 5 of Jones and plot the values of our flux tube radii $R(z)$ against height (keeping in mind that $k \simeq \pi/2R$) we see that they fall just inside the multicomponent region. Moreover, the height at which the flux tubes flare out coincides more or less with the thermalisation height of the K-line (see also Fig. 9 in Jones & Skumanich 1980), so that at heights where we should start to worry about lateral transfer in small-scale structures the tubes are no longer small in diameter.

Trujillo-Bueno & Kneer (1987) find that thermal variations on scales of even a few H can enhance the amplitude of radiative cooling in lines by an order of magnitude. Though it is difficult to relate their result directly to the other results described above, it does underline the extreme care with which multicomponent models should be interpreted.

4. Influence of model parameters on the K line

4.1. Influence of the temperature

The temperature structure of 2-D models influences the K line profile in a multitude of ways. Some of these effects are basic and are also found in 1-D models. Others are intrinsic to the particular geometry of 2-D models and indirectly due to the coupling of the geometry to the temperature field. The K-line source function is directly affected by the approximately exponential increase of electron density with temperature. Due to the concurrent increase in electronic collisions, the source function S_ν, therefore follows the local Planck function B_ν better in hotter atmospheres, as long as the continuum radiation field remains unchanged. This direct influence is mirrored by the range of profiles, shown in Fig. 4, produced by the 1-D atmospheric models FLUXT, VALP, VALF, and C′. These profiles at the same time represent the tube axis profiles from those 2-D models that include the above atmospheres in their magnetic region. To allow a better comparison with observations and spatially averaged profiles a macroturbulence of $6\,\mathrm{km\,s^{-1}}$ has been applied to each line profile (a VAL-like microturbulence is assumed). Note the logarithmic intensity scale.

The magnetic geometry only affects line profiles formed along rays passing through the magnetic canopy. The canopy base is

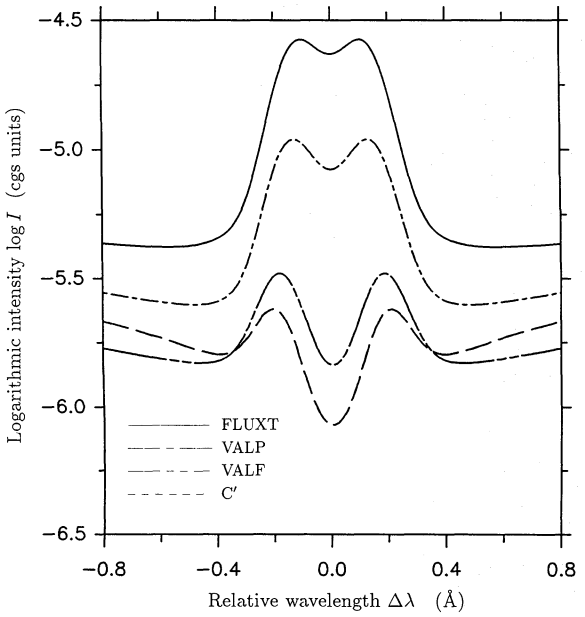

Fig. 4. Ca II K line logarithmic intensity, $\log I$, vs. relative wavelength, $\Delta\lambda$. Plotted are the cores of profiles resulting from the four empirical atmospheres used to represent the flux tube component. Solid curve: FLUXT, dot-dashed curve: VALP, dashed curve: C′, double-dot-dashed curve: VALF. The profiles correspond to those formed at the axes of symmetry of the fluxtubes with the respective atmospheres in the flux tube component. For example, the profiles formed at $r = 0$ of models A–D are (within numerically set limits) identical to the solid curve. The profiles have been concolved with a mactoturbulence of $6\,\mathrm{km\,s^{-1}}$. A VAL-like microturbulence, ξ_{mic}, is used for all models

associated with a jump in the temperature, density, electron density, etc. Therefore, the height of the canopy also affects the source function of the line directly. Also, the canopy base height itself depends on the temperature stratifications in the magnetic and non-magnetic regions (Solanki & Steiner 1990). This is an example of indirect coupling between geometry and temperature distribution in our models.

To study this coupling we now consider the K-line source function S_ν in greater detail. In Fig. 5 we show S_ν at various wavelengths between K_1 and K_3 (listed in the figure caption) as a function of $\log\tau$. In Fig. 5a and b we plot S_ν for rays 1 and 30 respectively, of model E, (ray 1 corresponds to the axis of the flux tube, i.e. to the network, ray 30 is representative of the interior of a supergranular cell). Similarly, in Fig. 5c and d we plot the source function for rays 1 and 30 of model J. Consider first the difference between Fig. 5a and c. The steeper temperature rise and hotter chromosphere of the VALP atmosphere in model E lead to an electron density almost an order of magnitude larger than in the VALF atmosphere and produce a stronger peak in S_ν just after it decouples from B_ν (note the different scales in Fig. 5a and c). Although the decoupling takes place at a larger optical depths in VALP than in VALF, the *geometrical depth* of decoupling is smaller in VALP than in VALF, because the H^- opacity increases sensitively with temperature. The continuum optical depths of the VALP (solid) and VALF (dashed) atmospheres are plotted vs. geometrical height in Fig. 6. Figures 5 and 6 show that, at the wavelength of K_2, the source function maximum occurs at approximately 1500 km for VALP and only at approximately 950 km for VALF. This difference plays an important role for the line profiles formed on rays that pass through the canopy. In Fig. 5b the presence of the canopy is signaled by the sudden rise in S_ν at approximately $\log\tau = -3.7$ after the steady decrease up to that point. The decoupling of S_ν from B_ν appears to happen at approximately the same continuum optical depth as for ray 1 of this model.

On the whole, S_ν changes quantitatively, but not qualitatively between rays 1 and 30 of model E. For model J, however, the difference is also qualitative. The chromospheric peak of S_ν has all but disappeared in Fig. 5d. The canopy now gives rise only to the small anomaly near $\log\tau = -5.2$, at a height at which S_ν and B_ν have long decoupled. For the FLUXT/COOLC combination (our model A) S_ν behaves in the same manner as in model E. The canopy lies even lower and the dethermalisation takes place at an even greater height, so that the presence of the canopy influences S_ν even less than in model E. The C′/COOLC combination (e.g., model Q) behaves qualitatively like model J.

The important point to bear in mind here is that a rise in chromospheric temperature, besides enhancing S_ν, raises the height at which S_ν reaches its chromospheric maximum and also lowers the height of the canopy base (quantified through the merging height, h_m, tabulated in Table 1). All these effects act in the same direction: they enhance the sensitivity to temperature of the K-line core of profiles formed in the canopy region in 2-D hydromagnetic models, compared to 1-D multicomponent models.

One way to illustrate the observable influence of changes in temperature in our models is to study a selected line parameter as a function of the radial distance from the axis of symmetry, r. As an example, the K_2 peak amplitude, normalized to the amplitude at $r = 0$, of five models (A, E, J, O, and Q) is plotted vs. r in Fig. 7.

Let us first discuss model O (C′/C′). Since the atmospheres in the magnetic and the non-magnetic regions of this model differ only by a vertical shift, no really significant variation is expected as a function of r. The variation that is seen in Fig. 7 can be explained by the inverse of the hot-wall effect observed in models of photospheric flux tubes (Spruit 1976; Knölker et al. 1988; Steiner & Stenflo 1990). The hot wall effect is due to the partial evacuation of flux tubes. This lowers their $\tau = 1$ level, allowing the non-magnetic atmosphere below the visible surface of the undisturbed photosphere to be seen through the walls of the flux tube. Since the temperature in the sub-photosphere increases rapidly with depth the walls appear disproportionately hot and bright. Such photospheric hot walls are also present in our models and cause a brightening of the continuum and of the K-line wings. Since photoionisation only plays a subordinate role in the formation of the K_2 feature, the photospheric hot walls do not affect the K_2 intensity. On the other hand, the K_2 source function, being coupled to the local temperature, reacts to any temperature jump at chromospheric heights. In model O the flux tube boundary passes through the approximate height of formation of K_2 in the C′ atmosphere (Uitenbroek 1989a) between $r \approx 300$ km and $r \approx 600$ km. Due to the positive outwards temperature gradient in the chromosphere the wall is cool there and this leads to the dip in K_2 intensity seen in Fig. 7. Once the wall has passed above the height of K_2 formation, the K_2 intensity of model O returns to the C′ value.

The other four models all have the same non-magnetic atmosphere, viz. COOLC. Model A has the hottest flux tube, produces the strongest K_2 peaks and shows the least variation of K_2 intensity with r. With decreasing temperature in the flux tube the horizontal variation in K_2 intensity increases rapidly. The discussion of the S_ν behaviour has already provided us with the main ingredients for explaining Fig. 7. For model A h_m lies below

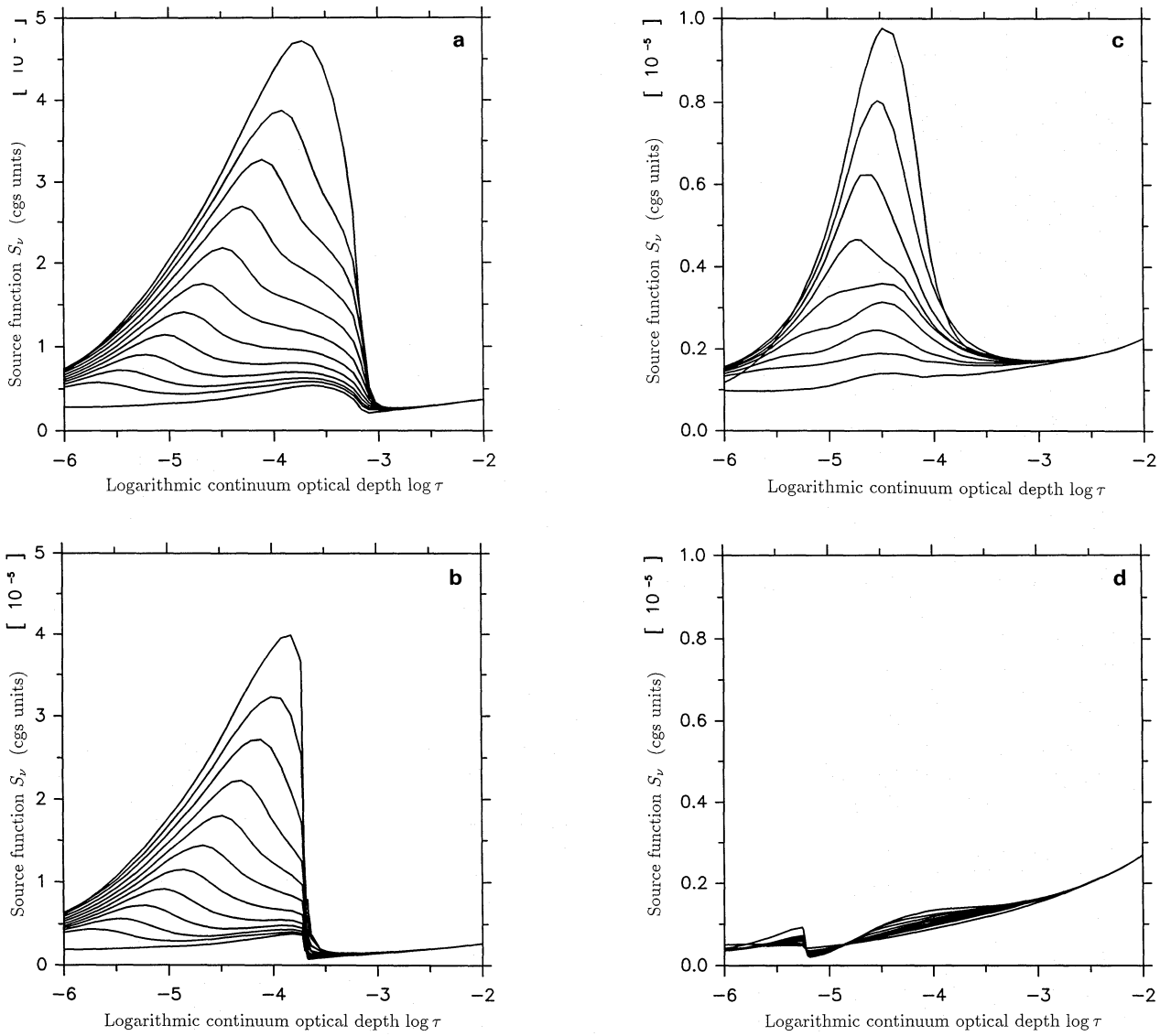

Fig. 5a–d. Source function, S_ν, at various wavelengths in the K line core vs. log τ. ξ_{mic} is VAL-like. **a** S_ν at the axis of model E (VALP/COOLC). From top to bottom the curves refer to wavelengths at 0.0, 0.145, 0.162, 0.178, 0.195, 0.212, 0.230, 0.248, 0.267, 0.287, 0.308, and 0.392 Å from line centre. **b** S_ν along ray 30 ($r \approx 1280$ km) of model E (VALP/COOLC). The curves refer to the same wavelengths as in **a. c** S_ν at the axis of model J (VALF/COOLC). From top to bottom the curves refer to wavelenghts at 0.0, 0.195, 0.212, 0.230, 0.248, 0.267, 0.287, 0.308, and 0.392 Å from line centre. **d** S_ν along ray 30 of model J. The curves refer to the same wavelengths as in **c**

the formation height of K_2 and at the bottom of the steep chromospheric increase of S_ν. Therefore, K_2 hardly feels the presence of the magnetic boundary and varies only minutely with r.

With decreasing temperature the canopy is moved up by up to 250 km for the models calculated here, but, more importantly, the chromospheric S_ν maximum and the formation height of K_2 are moved down by twice this amount (to a large part due to the temperature dependence of the optical depth scale). Therefore, for the cooler models K_2 is formed within the tube only near the tube axis. For larger r values it obtains considerable contribution from the cool atmosphere below the canopy.

Although for model A h_m lies below the formation height of K_2, it does not lie below the height from which the K_1 intensity originates. This may be seen from Fig. 8, where the line profiles formed at $r = 0$, $r = 265$ km and $r = 1280$ km are shown (to enhance the effect a microturbulence of only 2 km s^{-1} has been used for these calculations). Although wavelengths corewards of the K_2 peak remain virtually unaffected, the wingward wavelengths of the profiles formed along rays passing through the canopy have strongly suppressed intensities. For this model the presence of the canopy mainly makes the K-line emission core narrower and lowers the K_1 intensity. The lowering of the K_1 intensity for rays passing through the canopy is common to all the models with a COOLC non-magnetic atmosphere.

4.2. Influence of the field strength

The direct influence of the magnetic field on the unpolarized profile of the K line via the Zeeman effect is expected to be negligible. The K line has a relatively small Zeeman sensitivity. Its wings, formed in the photosphere in the presence of strong fields,

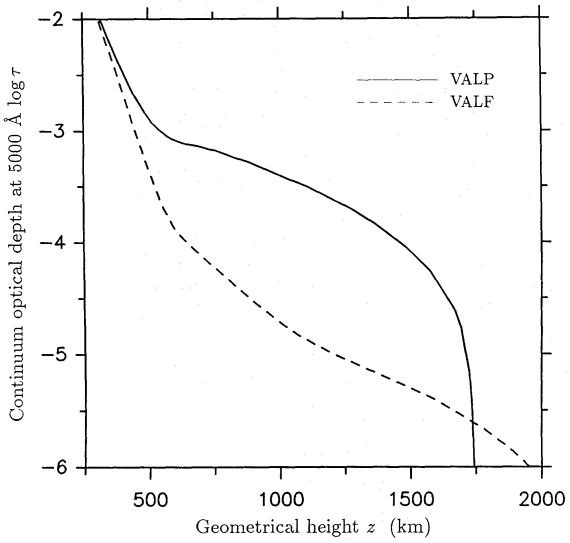

Fig. 6. Continuum $\log \tau_{5000}$ vs. geometrical height z for two atmospheres: VALP (solid) and VALF (dashed)

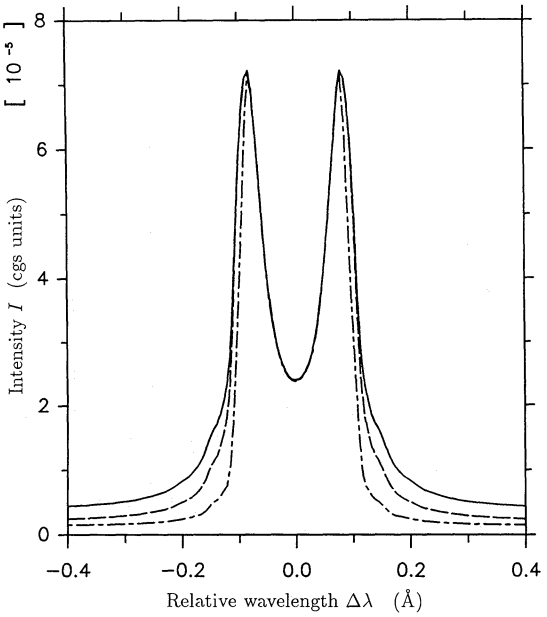

Fig. 8. K line profiles of model A at 3 different radii, r. Solid: $r = 0$, dashed: $r = 265$ km, dot-dashed: $r = 1280$ km. To enhance the difference in behaviour of K_1 and K_2 $\xi_{mic} = 2\,km\,s^{-1}$ and $\xi_{mac} = 0$ have been assumed

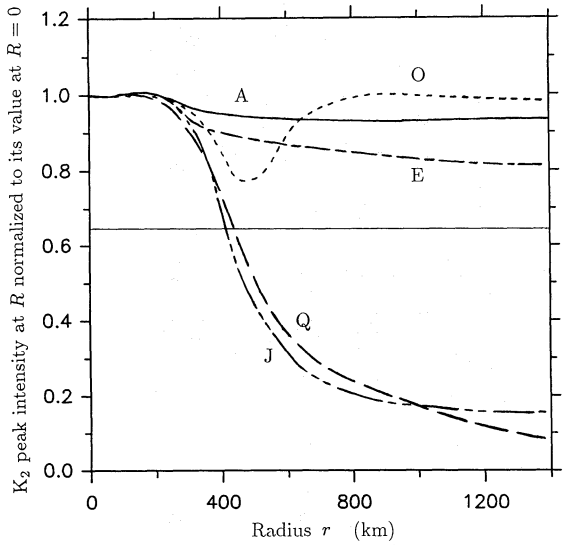

Fig. 7. Intensity of the K_2 peak at radius, r, normalized to its intensity at the flux tube axis ($r = 0$). Solid curve: model A (FLUXT/COOLC), dot-dashed curve: model E (VALP/COOLC), double-dot-dashed curve: model J (VALF/COOLC), dotted curve: model O (C′/C′), dashed curve: model Q (C′/COOLC). A VAL-like ξ_{mic} is assumed, $\xi_{mac} = 0$. The horizontal line marks the value to which the K_2 curves must drop at large r according to the observations of Grossmann-Doerth et al. (1974)

are so broad that they are completely unaffected, while the core is formed in the chromosphere where the field strength (outside sunspots) is small (< 250 G even for plages with a filling factor of 15% at $z = 0$, according to our models). Therefore, we have not included the Zeeman splitting in our calculations.

The magnetic free parameter of the models, B^*, corresponding to the field strength at $z = 0$, nevertheless affects those K line profiles formed along rays passing through the canopy. An increase in B^* shifts the canopy upwards (cf. Table 1) and the atmosphere within the magnetic feature downwards to achieve the increased evacuation required by horizontal pressure balance (Sect. 2). The downwards shift of the magnetic atmosphere, which basically implies an increase in the Wilson depression, is of a similar magnitude as the increase in h_m. In the photosphere this increases the temperature of the hot wall, so that the wing intensity of Ca II K can increase considerably in a thin ring around the flux tube axis. For sufficiently large field strengths even the K_1 intensity can be affected.

The influence of B^* on K_2 is illustrated in Fig. 9, where the radial dependence of the K_2 intensity is plotted for models E, F, and G ($B^* = 1500$ G, 1600 G, and 1630 G, respectively).[1] Due to its large formation height K_2 is only slightly affected by the hot wall. The intensity of K_2 at large r decreases considerably as B^* is increased. However, the difference at large r between the K_2 intensity of models E and G (different field strengths) is smaller than the difference between the K_2 intensity of models E and J (different temperatures) (Fig. 7), although models G and J have almost identical canopy heights. Keeping in mind that a part of the difference between the profiles resulting from models E and those from model G is due to the increased Wilson depression[2], the large difference between the line profiles from model E and from J implies that the major part of the change in radial dependence of the K_2 intensity produced by changing the temperature is due to

[1] Note, that although the three curves in Fig. 9 have been normalized to their values at $r = 0$, they still coincide at $r = 0$ if this normalisation is not carried out.

[2] An increase in B^* also means an increased evacuation above the canopy base. Close to h_m the gas pressure within and outside the magnetic region is almost the same (Solanki & Steiner, 1990). Since the temperature difference between the magnetic feature and the underlying CO clouds increases at h_m as B^* is increased, the gas density in the magnetic canopy must decrease.

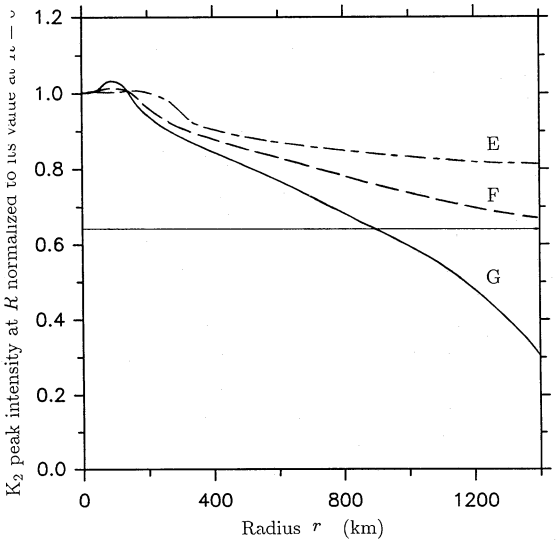

Fig. 9. K_2 peak intensity at radius r, normalized to its intensity at $r = 0$, plotted vs. r for three models with the same temperature (VALP/COOLC), but different field strength. Solid curve: model G ($B^* = 1630$ G), dashed curve: model F ($B^* = 1600$ G), dot-dashed curve: model E ($B^* = 1500$ G). B^* is the field strength at the flux tube axis at $z = 0$. ξ_{mic} is VAL-like. The horizontal line marks the value to which the K_2 curves must drop at large r according to the observations of Grossmann-Doerth et al. (1974)

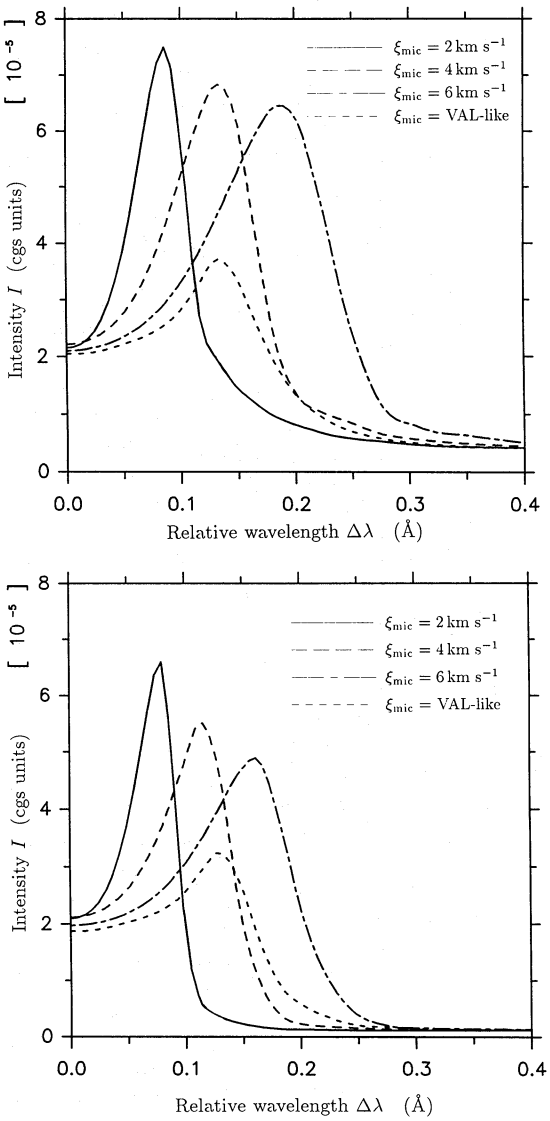

Fig. 10a and b. K line profiles for different microturbulences, ξ_{mic}. The macroturbulence is zero throughout. Solid curves: $\xi_{mic} = 2$ km s^{-1}, dashed: $\xi_{mic} = 4$ km s^{-1}, dot-dashed: $\xi_{mic} = 6$ km s^{-1}, dotted: VAL-like ξ_{mic}. **a** Profiles formed at the axis ($r = 0$) of model B. **b** Profiles formed at $r = 1280$ km of model B

the associated change in the thermalisation and formation depth. Therefore, Fig. 7 would not have changed dramatically, if the canopies of the various models were 100 km higher or lower than their calculated values, or if instead of calculating the canopies self-consistently we had kept a fixed canopy height of, say, 1000 km for models with $\alpha^* = 0.005$.

4.3. Influence of microturbulence and macroturbulence

We represent the non-thermal line broadening by a combination of micro- and macroturbulence. This velocity combination gives similar if not exactly the same profiles as stochastic meso-scale velocities (Carlsson & Scharmer 1985) and has the advantage of considerable simplicity.

Half profiles calculated along the central ray ($r = 0$) of model B with four different micro-turbulence velocities, ξ_{mic}, are shown in Fig. 10a (solid: $\xi_{mic} = 2$ km s^{-1}, dashed: $\xi_{mic} = 4$ km s^{-1}, dot-dashed: $\xi_{mic} = 6$ km s^{-1}, dotted: VAL-like). ξ_{mic} broadens the K_2 peaks, shifts them outwards and decreases their amplitudes. It leaves K_1 and K_3 practically unaffected. The detailed influence of a VAL-like ξ_{mic} on the K-line core has been discussed and explained in detail by Uitenbroek (1989a) and need not be dealt with again here.

For the present investigation it is of greater interest how the influence of the microturbulence on profiles formed at large r values compares to its influence on profiles at $r = 0$. Therefore, in Fig. 10b the profiles at $r = 1280$ km have been plotted for the same model and the same ξ_{mic} values as in Fig. 10a. Both atmospheric components are assumed to have the same ξ_{mic}. As the height independent ξ_{mic} increases, the difference between the profiles with r increases as well.

The effect of an increase in microturbulence is twofold. First, it broadens the local absorption profile, thereby changing the thermalisation of the line slightly. Secondly, it broadens the redistribution function, which changes the wavelength dependence of the PR line source function. The combination of these effects results in the difference in profiles displayed in Fig. 10. A narrow absorption profile (small microturbulence) decouples the core from the wings; the core source function follows the local Planck function to greater heights, leading to a higher chromospheric maximum, while the source function drops off faster with wavelength from line center because very few photons are fed into the inner wings from the core. Due to the broadened absorption profile the wavelength at which the source function maximum coincides with optical depth unity lies further and further from line center with increasing ξ_{mic}, shifting the peaks apart. The outward increase in the VAL-like microturbulence causes a plateau in the run of optical depth at those wavelengths where the Doppler core of the absorption profile goes over into the wing of the Voigt profile. The effect of this rise is that the chromospheric temperature rise is optically thin for K_2 photons. Coming from the inside the outward increase in width of the absorption profile will

shift K_2 photons just outside the Doppler core into the core so that they have to travel a large geometrical distance before their optical path to the outside world decreases. This reduces the contribution of the source function maximum to the emergent intensity, reducing the K_2 emission.

A macroturbulence, ξ_{mac}, reduces the intensity of the K_2 peaks, increases the full width at half maximum of the combined K_2 features and shifts the K_2 peaks. The direction of the shift depends on the ratio of the K_3 to K_1 intensity. If K_1 is stronger than K_3 (e.g. C′ model), then the peaks are shifted apart, but if K_3 is stronger than K_1 (e.g. FLUXT or VALP) the peaks are shifted closer together. Since the hotter models produce closer lying peaks anyway, ξ_{mac} tends to enhance this temperature effect.

In general the influence of ξ_{mic} on the radial dependence of the line profile is smaller than that of both the temperature and the field strength and plays only a minor role in determining Figs. 7 and 9. The influence of ξ_{mac} is almost independent of r, so that the curves in Fig. 7 and 9 are only slightly affected by ξ_{mac} as well. Therefore, although microturbulence and macroturbulence are required to reproduce the observed line profile shapes they introduce no new aspects to a 2-D treatment.

5. Comparison with observations

5.1. *Spatially resolved profiles*

Various observations suggest that the K line core brightness varies significantly on a scale of approximately 1″ (Bonnet et al. 1978; Cram & Damé 1983). It is at present unclear whether the K-line core varies on still smaller horizontal scales in the network or in plages. According to Athay (1986), the size of brightness structures increases steadily as the height of formation of the spectral diagnostic moves up from the photosphere into the chromosphere. For example Fang et al. (1984) and November & Ayres (private communication) find that K-line bright patches are considerably larger than the bright points observed cospatially in CN. We conclude from this that in order to reproduce the observed horizontal variation of K_2 brightness, our models must show a significant drop in intensity for $r \gtrsim 300$–500 km, but not necessarily for smaller r values.

The amplitude of the K-core intensity variation in quiet regions may be obtained from the statistical study of Grossmann-Doerth et al. (1974). They find an average K_2 brightness (normalized to the continuum) of approximately 9% at supergranule cell boundaries and somewhat less than 6% in the cell interiors (including what would be termed K_{2V} bright points and pure absorption profiles without readily distinguishable K_2 peaks). In summary, the average K_2 intensity in the cell interiors is slightly less than 2/3 the value in the network.

The observed value of Grossmann-Doerth et al. (1974) to which the synthetic K_2 curves must drop for $r \gtrsim 300$–500 km is marked by the horizontal line in Fig. 7. By comparing the calculated curves with the observed value for $r \gtrsim 500$ km we can roughly estimate the temperature within the magnetic features and directly also the associated canopy base height. The figure suggests that the temperature in the magnetic part of the chromosphere lies somewhere between that of VALP and VALF (if the external temperature is given by COOLC). The former model produces too little horizontal variation, while the latter appears to produce too much. Recalling that the radial dependence of the K_2 intensity (Grossmann-Doerth et al.) is also affected by the field strength, we have marked the observed average K_2 intensity in the cell centers (normalized to that in th network) in Fig. 9 as well (horizontal line). The relative level o horizontal K_2 intensity variation can be roughly reproduced b increasing B^* to 1630 G in the VALP/COOLC combinatio (model G). $B^* = 1630$ G corresponds to $\beta^* \approx 0.02$.

A comparison with Fig. 7 of Zayer et al. (1990), who plo empirically determined β values, suggests that a β^* of 0.02 can b considered a lower limit for small solar magnetic flux tubes an consequently $B^* = 1630$ G an upper limit, as long as COOLC describes the outer atmosphere.[1] The gradual decrease in K_2 intensity with r shown by model G in Fig. 9 contrasts with the rapid decrease between $r \approx 300$ km and $r \approx 600$ km shown by models J and Q in Fig. 7. Due to this gradual decrease model G cannot give rise to spatially well defined K_2 bright features at scales of 1″. Therefore, a cooler atmosphere within the flux tube, with a temperature between that of VALP and VALF, should give a better agreement with the observations.

5.2. *Spatially averaged profiles*

When comparing spatially averaged synthetic profiles from our 2-D models with low spatial resolution observations the main problem is the choise of magnetic filling factor at $z = 0$. Averaged over a couple of arc s, α^* on the Sun can vary by a factor of 50 or more between the quiet Sun and a strong plage (outside of sunspots). Since we have been unable to find observed K line *profiles* with a known α^*, we cannot reliably compare our average calculated profiles with measured profiles. Nevertheless, we roughly compare spatially averaged profiles of the models having $\alpha^* = 0.5\%$ with observations of the quiet Sun (we estimate the true α^* in the quiet Sun to lie between 0.1% and 1%), but do not attempt comparisons with spectrally resolved plage profiles.

Figure 11 shows the spatially averaged profiles resulting from models A, E, J, Q, and O. The profile produced by model O is almost identical to that resulting from the plane-parallel C′ atmosphere, which reproduces low spatial resolution observations in the quiet Sun very well (e.g. Ayres & Linsky 1976; Avrett 1985) and therefore serves as a proxy for the observations. All the profiles have been convoluted with a ξ_{mac} of 6 km s^{-1}.

It is clear from the figure that a temperature profile somewhere between that of model E and that of model J should reproduce the "observed" profile represented by C′ best. In view of the large differences between the model E line profile, respectively the model J profile and the C′ profile, it appears unlikely that the uncertainty in α^* can alone be responsible for the poor fits of either of the models to C′. For example, to make the K_2 intensity of model J match that of C′, α^* in model J would have to be larger than 5%, which is much too large for the quiet sun. Changing the field strength does not help sufficiently either. Raising B^* to 1630 G for the VALP/COOLC combination (model G) reduces the K_2 intensity by less than 0.2 compared to model E (in the units of Fig. 11).

A comparison of Fig. 4 with Fig. 11 shows that the spatially averaged profiles arising from the various models show larger relative differences than the profiles formed at the flux tube axes. This is a consequence of the heightened sensitivity of profiles

[1] We prefer to compare β^* rather than B^* with the observations, since the canopy height depends more directly on β^* than on B^* and for strongly evacuated tubes the relation between β^* and B^* depends strongly on the details of the *non*-magnetic atmosphere around $\tau = 1$.

ormed in the canopy to the temperature (cf. Sect. 4.1). Consequently, spatially averaged K line profiles from our 2-D models re more sensitive to the flux tube temperature than profiles from -D models.

In contrast to spectrally resolved line profiles, spectroheliograms of the K line core have been observed almost simultaneously with magnetograms. The relationship between K line core brightness and magnetic flux has been analysed by Skumanich et al. (1975) in the network and by Schrijver et al. (1989) in an active region plage. To test our models against this observational constraint we consider spatially averaged synthetic profiles (the observations of Skumanich et al. and Schrijver et al. were carried out with a pixel size of 2.″4), integrate their line core over a wavelength range of 1.04 Å (corresponding approximately to the photometer band-width used by Schrijver et al.) and divide the integral, I_c, by the intensity, I_w, at a wavelength 7.4 Å to the red of the core, again integrated over 1.04 Å. Following Schrijver et al., who normalized the core intensity by a wing intensity corresponding to the quiet Sun, we have used the I_w resulting from the C′ atmosphere to normalize all the I_c values.

We find when plotting I_c and I_w of single lines of sight vs. r for models with $\alpha^* = 0.5\%$, 5%, and 15% that for any given r value all three models give rise to almost identical I_c and I_w. This is to be expected, since below the merging height, the geometry of the flux tubes is nearly independent of the filling factor (Fig. 4 of Pneuman et al. 1986). Therefore, although we have only explicitly calculated models with $\alpha^* = 0.5\%$, 5%, and 15%, this excellent overlap allows us to determine I_c and I_w with high accuracy for other α^* values greater than 0.5% simply by adding together all the weighted profiles from a $\alpha^* = 0.5\%$ model, formed along rays at radial distances less than a given r_{max}, which corresponds to the desired α^*. The I_c/I_w values at $\alpha^* = 0$ have been obtained from profiles formed along a ray passing through the canopy far from the photospheric flux tube ($r = 1280$ km). In our models this mimics the situation when the observational aperture lies in the middle of a supergranule.

The resulting synthetic curves of I_c/I_w vs. α^* are shown in Fig. 12. The solid curves correspond to models with the VALF/COOLC combination, the dashed curves to the VALP/COOLC combination. The lower of each set of curves results for $B^* = 1630$ G, the upper for $B^* = 1500$ G. In order to avoid uncertainties in the exact spectral apparatus profile used by Schrijver et al. (we have assumed a rectangular form), uncertainties in converting the magnetogram signal into filling factor (cf. Grossmann-Doerth et al. 1987) and the influence on I_w of sizeable blends in the red K line wing, which we have not compensated for, we do not attempt a quantitative fit to the measured values at the present stage. Instead we see whether the models give a relationship between I_c/I_w and α^* similar in shape to that found by Schrijver et al. (1989). This also allows us to multiply the curves resulting from the VALF/COOLC combination by a factor of 3, thus enabling a better comparison between the results of the VALF/COOLC and the VALP/COOLC model combinations.

The asymptotic behaviour at large α^* of the synthetic curves in Fig. 12 is a natural result of our models and can be understood as follows: For small α^* (i.e. for profiles averaged over a large r value) the merging height is sufficiently high for the K line core to obtain a significant contribution from the cool underlying material. This lowers the core intensity by a large amount. The exact amount depends mainly on the temperature stratification (Sect. 4.1). As α^* is increased, h_m is lowered (cf. Table 1), so that the K line core obtains less and less contributions from the cooler non-magnetic atmosphere. Once the merging height has dropped sufficiently below the formation height of the Ca II core, the I_c/I_w index becomes independent of α^* (saturated), since any further increase in α^* does not change the atmosphere seen by the line core. Also, the larger the temperature, the lower the merging height for small α^* values and the larger the I_c/I_w there, so that I_c/I_w becomes asymptotic at smaller α^* values. This effect can be seen in Fig. 12 by comparing the dashed with the solid curves. For large α^* values all temperature stratifications used in the present paper (Table 1)

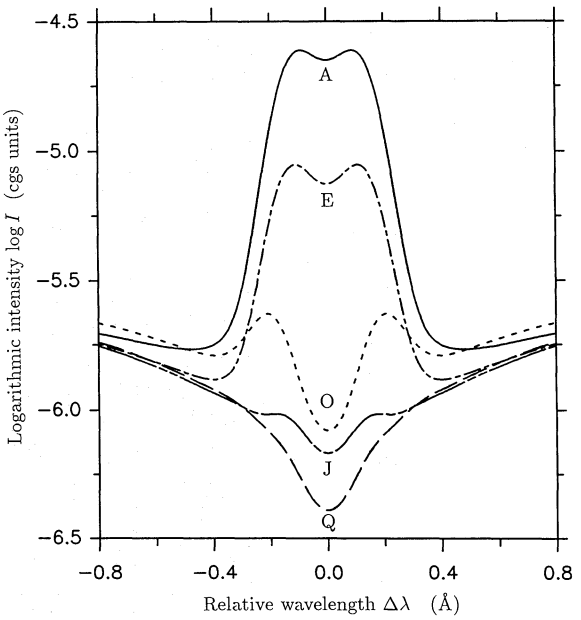

Fig. 11. Spatially averaged K line profiles for the models plotted in Fig. 7. All profiles have been calculated for a VAL-like ξ_{mic} and convolved with a macroturbulence of 6 km s^{-1}

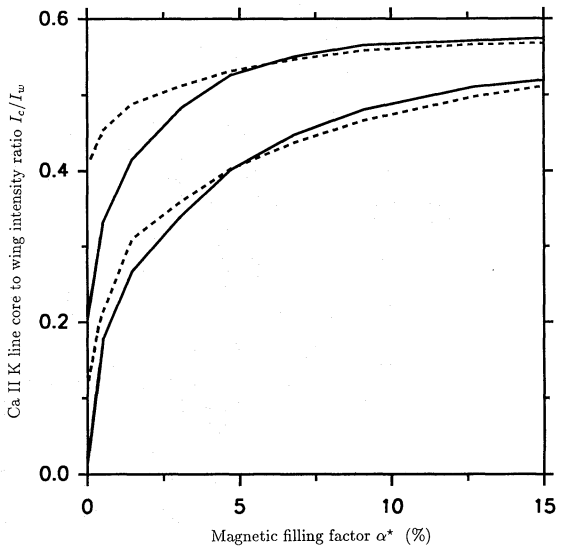

Fig. 12. K line core intensity normalized to the wing intensity, I_c/I_w, vs. magnetic filling factor, α^*. Solid curves: VALF/COOLC combination, dashed curves: VALP/COOLC combination. Lower two curves: $B^* = 1630$ G, upper two curves: $B^* = 1500$ G. For a better comparison between the models the curves resulting from the VALF/COOLC combination have been multiplied by a factor of 3. ξ_{mic} is VAL-like

give the same h_m and B^* plays the dominant role in fixing h_m. Therefore, the temperature stratification determines the *shape* of the I_c/I_w vs. α^* curve at the low α^* end, but B^* determines it for larger α^* values. However, note that the temperature does determine the *absolute value* of the curves for all α^* values. It is interesting that I_c/I_w does not disappear even at $\alpha^* = 0$. Our models, therefore, tend to show the presence of a "basal" flux, i.e. chromospheric emission, even when locally the magnetic filling factor in the photosphere is zero.

Qualitatively, the synthetic curves for $B^* = 1630$ G appear similar to the observations of Schrijver et al., with a steep initial rise followed by a gradual saturation for large α^*. Quantitatively there are differences, due probably both to the uncertainties in interpreting the observations mentioned above and the simplicity of our models. It must be stressed that our models give rise to a curves relationship between the line intensity and magnetic flux density quite naturally, without any need to vary the flux tube temperature as a function of the filling factor. It is interesting to note that, within the range of temperatures plotted here, the shape of the curves is determined more strongly by the field strength than by the temperature. In particular little difference is evident between the shapes of the two curves resulting from $B^* = 1630$ G. This suggests that we can predict with reasonable accuracy the form of the I_c/I_w vs. α^* curve for a temperature structure intermediate between VALP and VALF. Such a temperature structure is favoured by the other observations considered here.

6. Discussion and conclusion

We have presented the first line profile calculations in 2-D magnetohydrostatic models of the solar chromosphere. The main features of the models and of the line calculations are briefly summarized below:

(a) The magnetic field is structured in the form of vertical flux tubes in the solar photosphere. The field expands with increasing height and forms a canopy in the lower or middle chromosphere. The field represents a static, axially symmetric solution of the MHD equations.

(b) The magnetic features are hotter than the non-magnetic chromosphere, whose temperature corresponds to the COOLC model of Ayres et al. (1986). Except at the magnetic boundary there are no horizontal variations of the physical parameters of the atmosphere.

(c) The radiative transfer of the Ca II K line is carried out along numerous vertical rays passing through the model at different distances from the flux tube axis (1.5-D radiative transfer). A 5-level plus continuum representation of the Ca^+ ion is chosen and partial redistribution is allowed for.

Let us now briefly consider how well such model calculations fare when confronted with the six "basic" observations listed in Sect. 1.

1. Ca II K line profiles of the spatially averaged quiet Sun can be reproduced by a 2-D model having, besides a cool non-magnetic atmosphere (COOLC), a magnetic component with a temperature stratification between that of the VALF and the VALP atmospheres. The low K_1 intensity produced by the 2-D models suggests that the chromospheric temperature rise in magnetic features may have to be shifted to a lower altitude to reproduce the observations better.

2. In our 2-D treatment the amplitude of the horizontal variation of the K_2 intensity depends to a large extent on the temperature within the magnetic component. The amount of variation observed in the quiet Sun is reproduced by a flux tube temperature stratification between that of VALF and of VALP. These limits are consistent with those set by spatially averaged quiet Sun profiles (point 1 above). The approximate observed size of the K_2 bright network patches is also reproduced by our models. We have assumed a flux tube diameter of 200 km in the continuum forming layers.

3. The relation between the K line core intensity and magnetic flux, or rather Stokes V amplitude, observed by Skumanich et al. (1975) and Schrijver et al. (1989) can be qualitatively reproduced by the present models. Without changing any other parameter besides α^*, 2-D models produce both an initial steep increase in K line core brightness with filling factor and a leveling off at higher filling factors, as seen by Schrijver et al. (1989). In particular a curved relationship between K-line intensity and magnetic flux density is formed even though the atmospheric temperature/density structure is given a priori, regardless of, e.g., the filling factor. A temperature stratification between that of VALF and VALP is, once more, qualitatively consistent with the data. The models also produce a "basal" flux of Ca K core emission, even for a α^* very close to zero. The presence of such a "basal" flux has been deduced from observations by, e.g. Schrijver (1987) and Schrijver et al. (1989).

4. The reproduction of CO vibration-rotation fundamental band observations (Ayres & Testerman 1981; Ayres et al. 1986) requires temperatures below 4000 K in parts of the low chromosphere. Although we have not carried out explicit calculations, our 2-D models should automatically reproduce the CO line observations in the quiet Sun, since we include a cool atmosphere (COOLC) in the non-magnetic part of the model, which covers approximately 90% of the surface near the temperature minimum level for $\alpha^* = 0.5\%$. Such an area coverage by cool gas is comparable with the fraction assumed by Ayres et al. (1986). However, above the magnetic canopy the fraction of cool gas drops to 0%, in agreement with the conclusion of Athay & Dere (1990), that the chromospheric temperature rise is present over the whole solar surface.

5. If we accept that the temperature in the magnetic features lies between that of VALP and of VALF (points 1 and 2) and that the external temperature is given by COOLC (point 4) then we find that the canopy height in our models lies between 1000 and 1100 km above $z = 0$ in the quiet Sun ($\alpha^* = 0.5\%$). Although this height is considerably lower than most previous theoretical estimates (Gabriel 1976; Anzer & Galloway 1983), it is 200–400 km higher than the values inferred from magnetograms by Jones & Giovanelli (1983) in the quiet Sun. Solanki & Steiner (1990) were able to reproduce the observed height, but with a temperature within the magnetic component (FLUXT) which is too high to reproduce the Ca II K observations. We see three possible reasons for the discrepancy between the canopy height determined from magnetograms and from the Ca II K line.

(a) The canopy height determined by Jones and Giovanelli relies on the assumption that the chromosphere is thermally homogeneous. Their values may have to be revised if the inhomogeneity of the temperature is taken into account.

(b) One of the assumptions of the present analysis may be invalid. To our minds the most suspect assumption is that of horizontally constant temperature/density within the individual atmospheric components. It implies, for example, that synthetic transition region lines would not show any horizontal intensity variations in our 2-D models, for at this height the magnetic flux tube fills all the lateral space. This is contrary to observations. For example, Athay (1986) points out that the horizontal size of

nission structures remains approximately the same from the iiddle chromosphere to the transition zone. It is also difficult to ıvisage a heating mechanism which produces a homogeneous :mperature over the whole magnetic component, including the ırge canopy. By allowing a limited horizontal variation of the :mperature within the magnetic feature, we can, to a certain xtent, decouple the merging height from the temperature *above* ıe canopy base. In this way it may be possible to produce a low ying canopy and simultaneously a sizeable horizontal variation of he K line core intensity.

(c) The non-magnetic component of the chromosphere may ven be cooler than COOLC. For example, Solanki & Steiner 1990) found that the model combination C′/RE, where RE is the adiative equilibrium model of Anderson (1989), results in a nerging height of approximately 900 km. If we combine the VALF or the VALP atmospheres with the RE atmosphere, then he merging height ought to be even lower and should not differ oo strongly from the Jones and Giovanelli observations.

6. The present models take the intermittent nature of the magnetic field in the solar photosphere fully into account – the MHD code was originally developed to describe the structure and energetics of photospheric flux tubes. We have also chosen the photospheric free parameters of the models to correspond as closely as possible to observed values (cf. Sect. 2).

In the present paper we have not explicitly specified the source of the heating required to raise the chromospheric temperature above the radiative equilibrium value. Although at first sight it may appear that our models assume the heating to be exclusively of magnetic origin, this is not the case. Although a magnetic heating source is expected to mainly heat the magnetic component, the effect of a non-magnetic heating mechanism, e.g. acoustic waves, is less straight forward. We expect it to heat both the non-magnetic chromosphere and the magnetic canopy overlying it. There is theoretical evidence that in a CO cooled atmosphere acoustic waves become most effective close to the height of the magnetic canopy (Muchmore et al. 1989; cf. Solanki & Steiner 1990). Therefore, a hot magnetic canopy does not necessarily imply magnetic heating. Observationally there are strong indications for a mixed magnetic and non-magnetic origin of the heating, e.g., the "basal" flux in the Ca II H and K line cores, which is uncorrelated to magnetic activity (e.g. Schrijver 1987; Schrijver et al. 1989), and observational limits on the energy fluxes of MHD and acoustic waves (Solanki & Roberts 1990). According to our model the Ca II K core intensity never drops to values as low as those predicted by the COOLC model of Ayres et al., since even over the supergranule cell centers the K line core obtains some contribution from the hot magnetic canopy. This excess emission may be identified with the "basal" flux of Schrijver (cf. Fig. 12) and is probably due to the dissipation of acoustic waves.

Although multicomponent 1-D models (e.g. VAL 81, Avrett 1985; Ayres et al. 1986) can also reproduce some of the above observations, they have great difficulty reproducing all of them without introducing a large number of free parameters. Some observations, like that of the magnetic canopy, cannot be reproduced at all without at least a 2-D model. Since a 2-D model provides a means of introducing both hot and cool material along a single ray in a natural manner, it can overcome the problems associated with 1-D multicomponent models (cf. Sect. 1). Besides the small number of free parameters required to roughly reproduce a wide variaety of observations, the present models have the added advantage that they are based on solutions of the MHD equations and thus present a physically consistent picture of the chromosphere. However, we stress that the present calculations are far from definitive and leave ample scope for improvement and extension.

Acknowledgements. Listings of the atmospheric models FLUXT, COOLC and VALP were kindly provided by T. Ayres, for which we are very grateful. We also thank R. Rutten for valuable discussions and for his hospitality during the stay of one of us (SKS) in Utrecht. The remarks of the referee, C. Schrijver, which helped improve the presentation, are gratefully acknowledged. One of us (OS) acknowledges the financial support from the Swiss National Science Foundation, under grant No. 2000–5.229.

References

Anderson L.S., 1989, ApJ 339, 558
Anderson L.S., Athay R.G., 1989, ApJ 346, 1010
Anzer U., Galloway D.J., 1983, MNRAS 203, 637
Athay R.G., 1972, Radiation transport in spectral lines, Reidel, Dordrecht
Athay R.G., 1986, in: Physics of the Sun, Vol. II, ed. P.A. Sturrock et al., Reidel, Dordrecht, p. 51
Athay R.G., Dere K.P., 1990, ApJ 358, 710
Avrett E.H., 1985, in: Chromospheric Diagnostic and Modelling, ed. B.W. Lites, National Solar Obs., Sacramento Peak, NM, p. 67
Avrett E.H., 1990, in: Solar Photosphere: Structure, Convection, Magnetic Fields, ed. J.O. Stenflo, IAU Symp. 138, Kluwer, Dordrecht, p. 3
Avrett E.H., Loeser R., 1971, J. Quant. Spectrosc. Rad. Transf. 11, 559
Ayres T.R., Linsky J.L., 1976, ApJ 205, 874
Ayres T.R., Testerman L., 1981, ApJ 245, 1124
Ayres T.R., Testerman L., Brault J.W., 1986, ApJ 304, 542
Basri G.S., Linsky J.L., Bartoe J.-D.F., Brueckner G., Van Hoosier M.E., 1979, ApJ 230, 924
Bonnet R.M., Bruner E.C. Jr., Acton L.W., Brown W.A., Decaudin M., 1980, ApJ 237, L47
Bonnet R.M., Lemaire P., Vial J.C., Artzner G., Gouttebroze P., Jouchoux A., Leibacher J.W., Skumanich A., Vidal-Madjar A., 1978, ApJ 221, 1032
Bray R.J., Loughhead R.G., 1974, The solar chromosphere, Chapman and Hall, London
Bünte M., Steiner O., Solanki S.K., 1991, in: Solar Polarimetry, ed. L. November, National Solar Obs., Sacramento Peak, NM, p. 468
Carlsson M., Scharmer G.B., 1985, in: Chromospheric Diagnostic and Modelling, ed. B.W. Lites, National Solar Obs., Sacramento Peak, NM, p. 137
Chapman G.A., 1981, in: Solar Active Regions, ed. F.Q. Orall, Colorado University Press, p. 43
Cook J.W., Ewing J.A., 1990, ApJ 355, 719
Cram L.E., Damé L., 1983, ApJ 272, 355
Fang C., Mouradian Z., Banos G., Dumont S., Pecker J.C., 1984, Sol. Phys. 91, 61
Fiedler R.A.S., Cally P.S., 1990, Sol. Phys. 126, 69
Gabriel A.H., 1976, Phil. Trans. Roy. Soc. London A281, 339
Gingerich O., Noyes R.W., Kalkofen W., Cuny Y., 1971, Sol. Phys. 18, 347
Giovanelli R.G., 1980, Sol. Phys. 68, 49
Giovanelli R.G., Jones H.P., 1982, Sol. Phys. 79, 267
Gouttebroze P., 1986, A&A 160, 195

Gouttebroze P., Lemaire P., Vial, J.C., Artzner G., 1978, ApJ 225, 655
Grossmann-Doerth U., Kneer F., von Uexküll M., 1974, Sol. Phys. 37, 58
Grossmann-Doerth U., Knölker M., Schüssler M., Weishaar E., 1989, in: Solar and Stellar Granulation, eds. R.J. Rutten, G. Severino, Reidel, Dordrecht, p. 481
Grossmann-Doerth U., Pahlke K.-D., Schüssler M., 1987, A&A 176, 139
Jones H.P., 1986, in: Small Scale Magnetic Flux Concentrations in the Solar Photosphere, eds. W. Deinzer, M. Knölker, H.H. Voigt, Vandenhoeck and Ruprecht, Göttingen, p. 127
Jones H.P., Giovanelli R.G., 1983, Sol. Phys. 87, 37
Jones H.P., Skumanich A., 1980, ApJ 42, 221
Keller C.U., Solanki S.K., Steiner O., Stenflo J.O., 1990, A&A 233, 583
Knölker M., Schüssler M., Weisshaar E., 1988, A&A 194, 257
Knölker M., Grossmann-Doerth U., Schüssler M., Weisshaar E., 1991, Adv. Space Res. 11, 285
Lemaire P., Gouttebroze P., Vial J.C., Artzner G.E., 1981, A&A 103, 160
Lindsey C.A., Yee S., Roelling T.L., Hills R., Brock D., Duncan W., Watt G., Webster A., Jefferies J.T., 1990, ApJ 353, L53
Linsky J.L., 1985, in: Progress in Stellar Spectral Line Formation Theory, eds. J.E. Beckman, L. Crivellari, Reidel, Dordrecht, p. 1
Maltby P., Avrett E.H., Carlsson M., Kjeldseth-Moe O., Kurucz R.L., Loeser R., 1986, ApJ 306, 284
Mihalas D., Auer L.H., Mihalas B., 1978, ApJ 220, 1001
Owocki S.P., Auer L.H., 1980, ApJ 241, 448
Pneuman G.W., Solanki S.K., Stenflo J.O., 1986, A&A 154, 231
Scharmer G.B., Carlsson M., 1985, J. Comp. Phys. 59, 56
Schrijver C.J., 1987, A&A 172, 111
Schrijver C.J., Coté J., Zwaan C., Saar S.H., 1989, ApJ 337, 96
Shine R., Linsky J., 1974, Sol. Phys. 39, 49
Skumanich A., Smythe C., Frazier E.N., 1975, ApJ 200, 747
Solanki S.K., 1986, A&A 168, 311
Solanki S.K., 1989, A&A 224, 225
Solanki S.K., Roberts B., 1990, in: Solar Photosphere: Structure Convection, Magnetic Fields, ed. J.O. Stenflo, IAU Symp 138, Kluwer, Dordrecht, p. 259
Solanki S.K., Steiner O., 1990, A&A 234, 519
Spruit H.C., 1976, Sol. Phys. 50, 269
Steiner O., 1990, Ph.D. Thesis, ETH, Zürich
Steiner O., Pizzo V.J., 1989, A&A 211, 447
Steiner O., Pneuman G.W., Stenflo J.O., 1986, A&A 170, 126
Steiner O., Stenflo J.O., 1990, in: Solar Photosphere: Structure, Convection, Magnetic Fields, ed. J.O. Stenflo, IAU Symp. 138, Kluwer, Dordrecht, p. 181
Stenflo J.O., 1989, A&AR 1, 3
Stenholm L.G., Stenflo J.O., 1977, A&A 58, 273
Stenholm L.G., Stenflo J.O., 1978, A&A 67, 33
Trujillo-Bueno J., Kneer F., 1987, A&A 174, 183
Uitenbroek H., 1989a, A&A 213, 360
Uitenbroek H., 1989b, A&A 216, 310
Vernazza J.E., Avrett E.H., Loeser R., 1976, ApJS 30, 1
Vernazza J.E., Avrett E.H., Loeser R., 1981, ApJS 45, 635
Von der Lühe O., 1989, in: High Spatial Resolution Solar Observations, ed. O. Von der Lühe, Sacramento Peak, Sunspot, NM, p. 147
Zayer I., Solanki S.K., Stenflo J.O., 1989, A&A 211, 463
Zayer I., Solanki S.K., Stenflo J.O., Keller C.U., 1990, A&A 239, 356
Zirin H., 1988, Astrophysics of the Sun, Cambridge University Press, Cambridge